Supplementary Material:
Kinetics and mechanisms of stress relaxation in sputtered silver thin films

Quentin Hérault[a,1], Iryna Gozhyk[a], Matteo Balestrieri[a], Hervé Montigaud[a], Sergey Grachev[a], Rémi Lazzari[1,*]

[a]*Surface du Verre et Interfaces, UMR 125 CNRS/Saint-Gobain Recherche, 39 Quai Lucien Lefranc BP 135, F-93303 Aubervilliers, France*

[b]*CNRS, Sorbonne Université, Institut des NanoSciences de Paris, UMR 7588, 4 Place Jussieu, F-75005 Paris, France*

S1. Relaxation of evaporated/sputtered Ag/Mo films

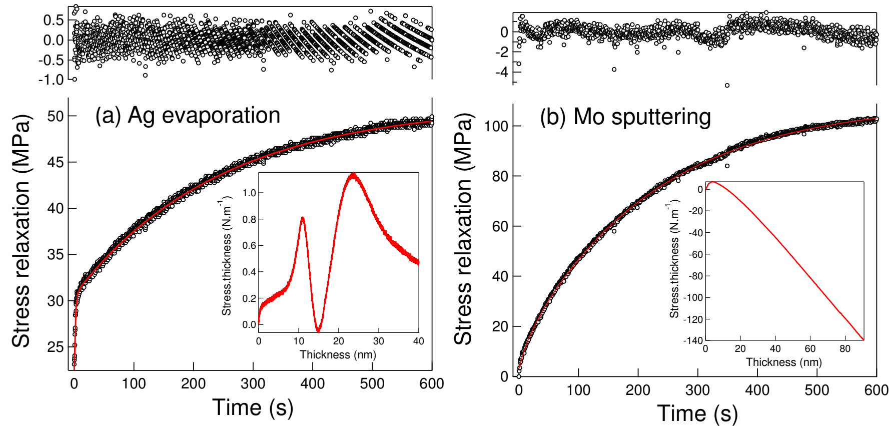

Figure S1: Post-growth stress relaxation (points) and its fit with two exponential terms for (a) a 40 nm evaporated film ($p = 10^{-4}$ μbar; $R = 0.033$ nm.s^{-1}) and (b) a 91 nm Mo sputtered film ($P = 150$ W; $p = 2$ μbar; $R = 0.28$ nm.s^{-1}). The insets show the corresponding stress.thickness evolution during growth; the puzzling initial evolution of stress.thickness for the evaporated film does not entail the conclusion *i.e.* the existence of only two exponential components of stress relaxation.

*Corresponding author

Email addresses: quentin.herault@saint-gobain.com (Quentin Hérault), iryna.gozhyk@saint-gobain.com (Iryna Gozhyk), matteo.balestrieri@saint-gobain.com (Matteo Balestrieri), herve.montigaud@saint-gobain.com (Hervé Montigaud), sergey.grachev@saint-gobain.com (Sergey Grachev), remi.lazzari@insp.jussieu.fr (Rémi Lazzari)

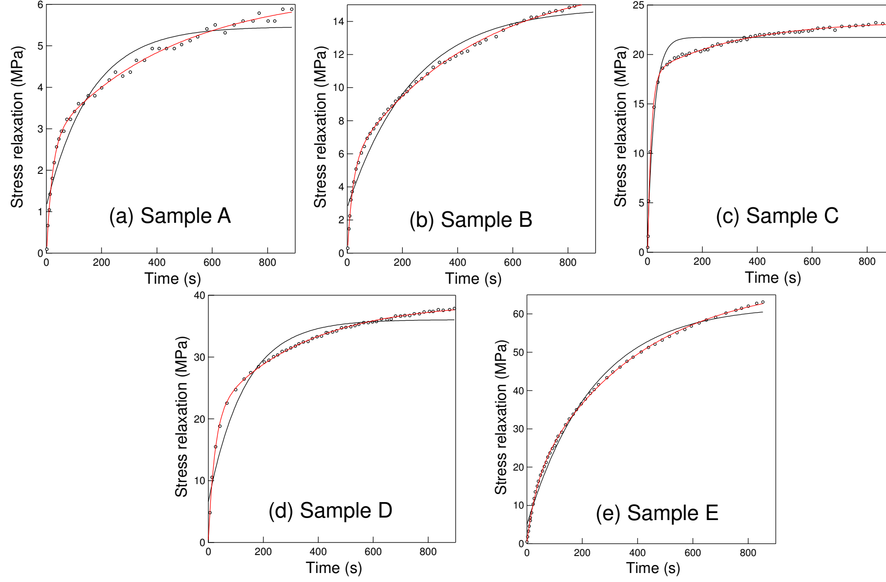

Figure S2: Fits of the stress relaxation data of Fig. 3 of reference [1] for a 145 nm thick evaporated Ag films with one (black line) and two (red line) exponential components. The substrate is a Si wafer similar to that used in the present study. To achieve different grain sizes, sample A-E have been grown either at low ($R = 0.034$ nm.s^{-1}; samples A,B,E) or fast ($R = 0.618$ nm.s^{-1}; samples C,D) deposition rates. The samples differ also by the presence (sample E,D) or absence (sample A,B,C) of a Ge seed layer. Only the first growth/relaxation cycle of reference [1] has been analysed. Note that, according to authors, data are already corrected for thermal stress. Better fits are achieved with two exponential terms.

S2. Modelling of temperature evolution during sputtering deposition

Unlike evaporation, magnetron sputtering deposition involves highly energetic species of different origins (electrons, ions, neutral atoms, photons) that may contribute to sample heating [3–10]. It is well known that the power supply type (radio-frequency or direct-current) and other deposition parameters (power, pressure, substrate-target distance, sample polarization etc. . .) strongly determine the incoming species and their relative energies [10]. Reaching several hundreds of degrees in extreme cases [9] like during plasma etching [11], the temperature rise can not be neglected when studying thin film mechanical properties even in less harsh environments. This phenomenon gives rise to the so-called thermal stress, which is due to different thermal expansion coefficients between the film and the substrate [12–16]. To get insight into the evolution of this stress component, a heat exchange model of the temperature evolution [3–9, 11] is developed herein and compared to actual temperature measurements (see Section 3.3 of the article).

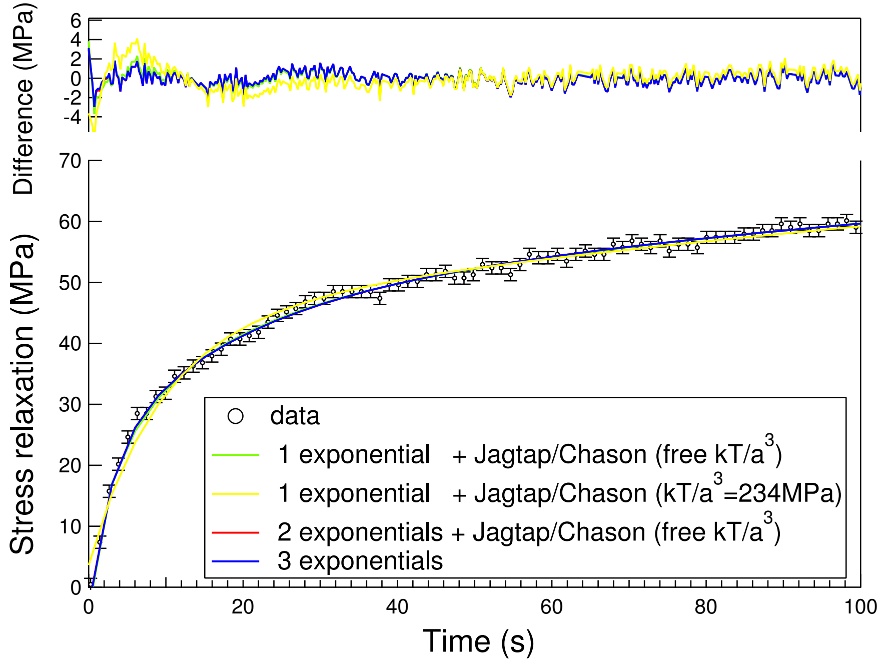

Figure S3: Fits of stress relaxation of sputtered Ag film ($P = 50$ W; $p = 2$ μbar): comparison between exponential (blue line; Eq. 2 of the article) and refined stress relaxation $\Delta\overline{\sigma}_{gb}(t) = \Delta\overline{\sigma}_{gb} + \frac{kT}{a^3} \ln\left[1 - \left(1 - e^{-\frac{\Delta\overline{\sigma}_{gb} a^3}{kT}}\right) e^{-t/\tau_{gb}}\right]$ (Eq. 12 of Reference [2]; green, yellow and red lines) to account for the mechanism of out-diffusion of atoms from GBs. One (green and yellow lines) or two exponentials (red and blue lines) terms are added to describe thermal stress $\Delta\overline{\sigma}_{th}$ and GB grooving $\Delta\overline{\sigma}_{surf}$. No difference is observed in terms of agreement between data and different modellings (green, red and blue lines) except for the fit with a fixed value of $\frac{kT}{a^3} = 234$ MPa value (yellow line) for which the difference is similar to a fit with only two exponentials (see Fig. 3 of the article). However, the model of Reference [2] combined with thermal stress (green line) but with a free $\frac{kT}{a^3}$ parameter leads to unreasonable values of $\Delta\overline{\sigma}_{gb} \simeq 50$ MPa and of $\frac{kT}{a^3} \simeq 17.5$ MPa one order of magnitude lower than expectation with $\tau_{gb} \simeq 21.5$ s. At the opposite combined with two extra-exponential terms, the model of Reference [2] (red line) gives $\frac{kT}{a^3} \simeq 270$ MPa, $\Delta\overline{\sigma}_{gb} \simeq 23.8$ MPa and $\tau_{gb} \simeq 3$ s in close agreement with expectation and values obtained with three exponentials (blue line; $\Delta\overline{\sigma}_{gb} \simeq 26.2$ MPa and $\tau_{gb} \simeq 3.7$ s). Indeed, the refined model of Reference [2] reverts to a simple exponential term through an expansion to first order in the small relaxation amplitude $\Delta\overline{\sigma}_{gb} a^3/kT = 0.09$.

The average substrate-layer temperature T_s results from a complex balance between heating sources, cooling phenomena and thermal capacity. It obeys the following equation:

$$C_s \frac{dT_s}{dt}(t) = \Phi_{in} - \Phi_{out}, \tag{S1}$$

where Φ_{in} is the incoming flux of energy related to deposition and to the presence of a plasma, Φ_{out} the outgoing one and C_s the thermal capacity of the wafer.

Φ_{in} depends not only on the deposition rate of neutral atoms through various energetic terms (condensation energy, kinetic energy, re-sputtered species energy, plasma energy), but also on the energy flux of charged species hitting the substrate (electrons and ions) and of plasma induced radiation [5–9]. All these contributions change with deposition conditions in a complex way so that the exact value of Φ_{in} is hardly predictable during magnetron sputtering process [10]. However, all contributions can be assumed to be constant and independent of temperature for a given set of growth parameters, and, of course, equal to zero during post-deposition relaxation. Φ_{out} depends on the substrate temperature through three components: (i) thermal radiation, (ii) heat transfer through the sample holder and (iii) conduction through the sputtering gas:

$$\Phi_{out} = \Phi_{rad} + \Phi_{cond-s} + \Phi_{cond-g}. \tag{S2}$$

The radiation loss can be written using the Stefan-Boltzmann law [7] as the sum of the radiation loss from the film side and that from the back of the substrate:

$$\Phi_{rad} = A_s \sigma (\epsilon_f + \epsilon_s)[T_s^4(t) - T_c^4]. \tag{S3}$$

A_s is the surface of the substrate, σ the Stefan-Boltzmann constant, T_c the temperature of the chamber walls and ϵ_f, ϵ_s the emissivities of the film and the substrate. Eq. S3 implies that the deposition occurs on one face of the wafer and that the emissivity on the film side does not change with time (which is true during post-deposition relaxation of a continuous film). Part of the thermal loss, Φ_{cond-s}, is due to the contact between the substrate and its sample holder (herein via the surface of the three tiny pins). As thermocouple measurements showed a constant holder temperature $T_h \simeq T_c$ over time, the outgoing flux due to solid conduction is given by the Fourier law [7]:

$$\Phi_{cond-s} = \frac{1}{R_{th}} \left[T_s(t) - T_h \right], \tag{S4}$$

where R_{th} is substrate/holder thermal resistance. Finally, thermal losses due to the sputtering gas, Φ_{cond-g}, change with pressure p. During relaxation, this phenomenon involves both faces of the substrate, but only its rear face during growth, since the energy transfer through the impinging Ar atoms on the plasma side are already implicitly included in the net Φ_{in} term. For a gas temperature $T_g \simeq T_c$ close to that of the chamber walls, the conduction term reads [7]:

$$\Phi_{cond-g} = \eta \alpha \Lambda_0 p A_s \left[T_s(t) - T_g \right], \tag{S5}$$

where η is the number of faces prone to cooling (1 for deposition and 2 for relaxation measurement), α an accommodation coefficient (between 0 and 1) related to the fraction of transferred energy between an impinging atom and the surface, and Λ_0 the gas thermal conductivity. Eq. S5 is valid in the free molecular regime, *i.e.* if the gas atom mean free path λ_g is larger than or comparable to the cathode sheath thickness d_{st}. In the present explored pressure range for Ar ($p = 2 - 50$ μbar), $\lambda_g = 0.7 - 3.5$ cm while $d_s \approx 1$ cm [7].

Before trying to solve Eq. S1, it is worth evaluating the orders of magnitude of the three heat loss terms Φ_{rad} (Eq. S3), Φ_{cond-s} (Eq. S4) and Φ_{cond-g} (Eq. S5). As it is shown in the article, an increase of about 20 K for a final 40 nm thick Ag film on Si will be assumed in the calculation with the following set of parameters: $A_s = 20$ cm^2; $\sigma = 5.67\,10^{-8}$ W.m^{-2}.K^{-4}; $\epsilon_f = 0.02$; $\epsilon_s = 0.6$; $T_c = T_h = T_g = 293$ K; $R_{th} = 500$ K.W^{-1}; $\alpha = 0.5$; $\Lambda_0 = 0.332$ W.m^{-2}.K^{-1}.Pa^{-1} for Ar; $p = 50$ μbar. The calculated values $\Phi_{rad} \simeq 1.6\,10^{-1}$ W, $\Phi_{cond-s} \simeq 4.0\,10^{-2}$ W and $\Phi_{cond-g} \simeq 3.3\,10^{-2}$ W show that none of the heat loss components is really negligible.

In order to derive the temporal evolution of the temperature, some approximations are necessary. By assuming a small difference $\Delta T_s(t) = T_s(t) - T_c$, the Stefan-Boltzmann law can be linearised:

$$\Phi_{rad} = 4A_s(\epsilon_f + \epsilon_s)\sigma T_c^3 \Delta T_s(t). \tag{S6}$$

With this first order expansion, the thermal balance (Eq. S2) finally reads:

$$\frac{dT_s}{dt}(t) + \frac{1}{\tau_T} T_s(t) = \frac{1}{C_s}(\Phi_{in} + \Phi_0), \tag{S7}$$

where

$$\frac{1}{\tau_T} = \frac{1}{C_s}\left[4A_s\sigma(\epsilon_f + \epsilon_s)T_c^3 + \frac{1}{R_{th}} + \eta A_s \alpha \Lambda_0 p\right] \tag{S8}$$

$$\Phi_0 = 4A_s\sigma(\epsilon_f + \epsilon_s)T_c^4 + \frac{T_h}{R_{th}} + \eta A_s \alpha \Lambda_0 p T_g \simeq \frac{C_s}{\tau_T} T_c. \tag{S9}$$

The above equation is valid both for deposition ($\eta = 1, \Phi_{in}$ =constant) and during relaxation ($\eta = 2, \Phi_{in} = 0$). Assuming a constant Φ_{in} term during growth, the temperature $T_{heat}(t)$ rises following an exponential behaviour:

$$\begin{aligned} T_{heat}(t) &= T_h + \Delta T_{heat}^{\infty}\left[1 - \exp\left(-t/\tau_T\right)\right] \\ \Delta T_{heat}^{\infty} &\simeq \frac{\tau_T}{C_s}\Phi_{in}, \end{aligned} \tag{S10}$$

with a time constant τ_T given by Eq. S8. Similarly, the temperature during cool-down $T_{cool}(t)$ follows an exponential decay during relaxation after growth:

$$T_{cool}(t) = T_{end} - (T_{end} - T_h)\left[1 - \exp\left(-t/\tau_T\right)\right], \tag{S11}$$

where T_{end} is the final temperature reached at the end of deposition.

S3. Exponential behaviours of stress relaxation in case of grain boundary grooving

The general equation of the average stress evolution [17–19] (Eq. 6 of the manuscript) in the case of stress generation by diffusion of atoms in grain boundaries (GB) can be recasted into an "exponential-like" differential equation:

$$\frac{\partial \overline{\sigma}}{\partial t} = -\frac{\overline{\sigma}}{\tau_{eff}} + \sigma_\infty, \tag{S12}$$

with an effective time constant given by:

$$\frac{1}{\tau_{eff}} = \frac{a}{h\tau} + \frac{1}{h}\frac{\partial h}{\partial t}, \tag{S13}$$

and a limit value:

$$\sigma_\infty = \sigma_C + \frac{\tau}{a}\frac{\partial h}{\partial t}\sigma_T. \tag{S14}$$

In the case of a relaxation process involving GB grooving, the initial condition is $\overline{\sigma}(t=0) = \sigma_{ss}$ and, since $\lim_{t\to\infty} \frac{\partial h}{\partial t} = 0$, $\lim_{t\to\infty} \overline{\sigma} = \sigma_C$.

In the case of an exponential GB grooving (Eq. 10 of the manuscript) slower than the diffusion of atoms in GBs, *i.e.* $\tau/a \ll \tau_{gv}/\Delta h_f$, $\tau_{eff} \simeq \frac{h\tau}{a}$ decays slowly by a factor $(h_f - \Delta h)/h_f$. Therefore, if $\Delta h_f \ll h_f$, the relaxation follows initially a fast exponential behaviour of time constant $\tau_{gb} = \frac{h_f}{a}\tau$ with an amplitude:

$$\Delta\overline{\sigma}_{gb} = \sigma_C + \frac{\tau}{a}\left(\frac{\partial h}{\partial t}\right)_{t=0}\sigma_T - \sigma_{ss} = \sigma_C - \frac{\tau}{\tau_{gv}}\frac{\Delta h}{a} - \sigma_{ss}, \tag{S15}$$

but with a limit value σ_∞ (Eq. S14) that will drift slowly and exponentially as $\frac{\partial h}{\partial t}$ with a time constant τ_{gv} and an amplitude:

$$\Delta\overline{\sigma}_{surf} = \frac{\tau}{\tau_{gv}}\frac{\Delta h}{a}. \tag{S16}$$

Therefore, the evolution of $\overline{\sigma}$ can be decomposed into two exponential terms with fast $\tau_{gb} = \frac{h}{a}\tau$ and slow $\tau_{surf} = \tau_{gv}$ time constants corresponding to the two underlying mechanisms of out-diffusion of atoms from GBs and GB grooving. While the former exponential component scales linearly with the initial σ_{ss} value, the latter has a constant amplitude.

At the opposite limit of the time scale, *i.e.* $\tau/a \gg \tau_{gv}/\Delta h_f$, as shown by Eq. S13, the stress evolution (Eq. 10 of the manuscript) is dominated by the fast term $\frac{\partial \overline{\Sigma}_{gr}}{\partial t}$ for a short time before switching to a slower one $\frac{\partial \overline{\Sigma}_{gb}}{\partial t}$ and reaching the final σ_C value. The amplitude of the two terms have opposite sign. Inserting

the following exponential behaviours:

$$\overline{\Sigma}_{gb} = \sigma_C - \Delta\sigma_{gb} \exp\left(-\frac{at}{h_f \tau}\right)$$
$$\overline{\Sigma}_{gr} = -\Delta\sigma_{surf} \exp\left(-\frac{t}{\tau_{gv}}\right) \quad \text{(S17)}$$

into the differential equation Eq. 10 and taking the $t = 0$ limit, one finds a first linear equation between the two amplitudes. By combing this equation with the initial condition $\overline{\sigma}(t = 0) = \sigma_{ss}$, one finds:

$$\Delta\sigma_{gb} = \frac{h_f + \Delta h}{h_f}(\sigma_C - \sigma_{ss}) + \frac{\Delta h}{h_f}\sigma_T \quad \text{(S18)}$$

$$\Delta\sigma_{surf} = -\frac{\Delta h}{h_f}(\sigma_C - \sigma_{ss}) - \frac{\Delta h}{h_f}\sigma_T. \quad \text{(S19)}$$

Being of different signs (see Fig. 9-b of the article), both exponential amplitudes scale with the steady-state stress σ_{ss}.

S4. Steady-state stress and relaxation time versus deposition conditions

The kinetic model of Chason [17–19] of stress evolution during growth is based on a competition between tensile stress $\sigma_T > 0$ due to GB zipping and compressive stress $\sigma_C < 0$ due to atom incorporation along GBs driven by the difference of chemical potential between the surface and the interior of GBs. In the case of fast diffusion along GBs, the models predict the following link between the steady-state stress σ_{ss} and the introduced characteristic time constant τ :

$$\sigma_{ss} = \frac{\sigma_T + \frac{a}{R\tau}\sigma_C}{1 + \frac{a}{R\tau}} \quad \text{(S20)}$$

where a^3 ($a = 0.257$ nm) is the atomic volume and R the growth rate. At the opposite limit of slow diffusion with atom incorporation limited to the top part of GBs,

$$\sigma_{ss} = \sigma_C + (\sigma_T - \sigma_C)\exp\left(-a/R\tau\right). \quad \text{(S21)}$$

τ scale with the grain size and is also linked to the post-growth relaxation time τ_{gb} as measured in this work by $\tau = \frac{a}{h_f}\tau_{gb}$ (respectively, $\tau = \tau_{gb}$) in the fast (respectively, slow) diffusion hypothesis. A check of a linearised version of Eq. S20-S21 is shown in Fig. S4 for all studied sputtering deposition conditions. If the linear trend is better fulfilled for fast diffusion with $\sigma_C < 0$, both fits give non-physical negative tensile σ_T values.

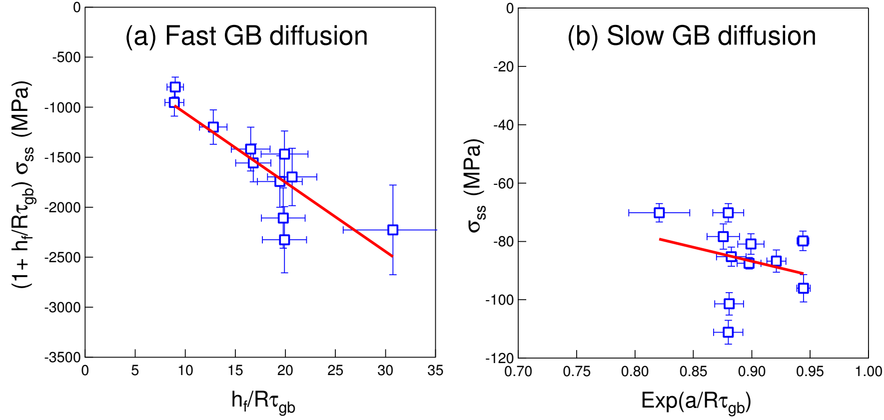

Figure S4: Check of the predictions of the kinetic model of stress evolution for the steady-stress in (a) the fast (Eq. S20) and (b) slow (Eq. S21) diffusion regimes.

References

[1] D. Flötotto, Z. M. Wang, L. P. H. Jeurgens, E. J. Mittemeijer, Kinetics and magnitude of the reversible stress evolution during polycrystalline film growth interruptions, J. Appl. Phys. 118 (2015) 055305.

[2] P. Jagtap, E. Chason, A unified kinetic model for stress relaxation and recovery during and after growth interruptions in polycrystalline thin films, Acta Materialia 193 (2020) 202–209.

[3] J. A. Thornton, Substrate heating in cylindrical magnetron sputtering sources, Thin Solid Films 54 (1978) 23–31.

[4] J. A. Thornton, J. L. Lamb, Substrate heating rates for planar and cylindrical-post magnetron sputtering sources, Thin Solid Films 119 (1984) 87–95.

[5] R. Wendt, K. Ellmer, K. Wiesemann, Thermal power at a substrate during ZnO:Al thin film deposition in a planar magnetron sputtering system, J. Appl. Phys. 82 (1997) 2115–2122.

[6] H. Kersten, G. M. W. Kroesen, R. Hippler, On the energy influx to the substrate during sputter deposition of thin aluminium films, Thin Solid Films 332 (1) (1998) 282–289.

[7] H. Kersten, H. Deutsch, H. Steffen, G. M. W. Kroesen, R. Hippler, The energy balance at substrate surfaces during plasma processing, Vacuum 63 (2001) 385–431.

[8] S. D. Ekpe, S. K. Dew, Theoretical and experimental determination of the energy flux during magnetron sputter deposition onto an unbiased substrate, J. Vac. Sci. Technol., A 21 (2003) 476–483.

[9] J. G. Han, Recent progress in thin film processing by magnetron sputtering with plasma diagnostics, J. Phys. D: Appl. Phys. 42 (2009) 043001.

[10] D. Depla, S. Mahieu, Reactive Sputter Deposition, Springer, Berlin, Heidelberg, 2008.

[11] J. F. Daviet, L. Peccoud, F. Mondon, Heat transfer in a microelectronics plasma reactor, J. Appl. Phys. 73 (1993) 1471–1479.

[12] R. Abermann, H. P. Martinz, R. Kramer, Thermal effects during the deposition of thin silver, gold and copper films and their influence on internal stress measurements, Thin Solid Films 70 (1980) 127–137.

[13] L. B. Freund, S. Suresh, Thin film materials: stress, defect formation and surface evolution, Cambridge University Press, 2004.

[14] R. Koch, D. Winau, A. Führmann, K. H. Rieder, Growth-mode-specific intrinsic stress of thin silver films, Phys. Rev. B 44 (1991) 3369–3372.

[15] R. Koch, R. Abermann, On the influence of thermal effects on internal stress measurements during and after deposition of silver, gold and copper films, Thin Solid Films 129 (1985) 63–70.

[16] E. Chason, P. R. Guduru, Tutorial: understanding residual stress in polycristalline thin films through real-time measurements and physical models, J. Appl. Phys. 119 (2016) 191101.

[17] E. Chason, B. W. Sheldon, L. B. Freund, J. A. Floro, S. J. Hearne, Origin of compressive residual stress in polycrystalline thin films, Phys. Rev. Lett. 88 (2002) 156103.

[18] E. Chason, A kinetic analysis of residual stress evolution in polycrystalline thin films, Thin Solid Films 526 (2012) 1 – 14.

[19] E. Chason, J. W. Shin, S. J. Hearne, L. B. Freund, Kinetic model for dependence of thin film stress on growth rate, temperature, and microstructure, J. Appl. Phys. 111 (8) (2012) 083520.